

A Study on Plasma Formation on Hypersonic Vehicles using Computational Fluid Dynamics

Original

A Study on Plasma Formation on Hypersonic Vehicles using Computational Fluid Dynamics / Esposito, S.; D'Ambrosio, Domenic. - ELETTRONICO. - (2023). (Intervento presentato al convegno Aerospace Europe Conference 2023 – 10 EUCASS – 9 CEAS tenutosi a Lausanne, Switzerland nel 9-13 July, 2023) [10.13009/eucass2023-492].

Availability:

This version is available at: 11583/2985003 since: 2024-01-12T13:12:18Z

Publisher:

EUCASS

Published

DOI:10.13009/eucass2023-492

Terms of use:

This article is made available under terms and conditions as specified in the corresponding bibliographic description in the repository

Publisher copyright

(Article begins on next page)

A Study on Plasma Formation on Hypersonic Vehicles using Computational Fluid Dynamics

Salvatore Esposito[†] and Domenic D'Ambrosio
Politecnico di Torino
Corso Duca degli Abruzzi 24, 10129, Torino, Italy
salvatore_esposito@polito.it · domenic.dambrosio@polito.it
[†]Corresponding author

Abstract

This study focuses on understanding high-temperature effects and plasma formation in sub-orbital hypersonic flight using Computational Fluid Dynamics (CFD) simulations. The research compares two models with different kinetic parameters derived from shock tube experiments and state-to-state chemical kinetics. The simulations consider various Mach numbers and altitudes relevant to reentry conditions. Results show that the choice of model and the number of species composing the mixture significantly impact the flow field, with the more recent model demonstrating improved accuracy compared to experimental and numerical data.

1. Introduction

Hypersonic flight refers to a particular flight regime in which objects travel through the atmosphere at high supersonic speeds, typically above Mach 5, subjecting them to a unique set of physical phenomena. An object traveling at hypervelocity transfers its kinetic energy to the air through a detached shock wave, which compresses and heats the gas, increasing its internal energy. These high temperatures trigger chemical reactions between gas species, changing the characteristics of the flow field and leading to phenomena such as internal energy redistribution, dissociation, and ionization, most of which occur in non-equilibrium conditions. An accurate description of these effects is essential for predicting the thermal loads experienced by the aircraft for design and operation in a hypersonic flight mission. In addition, if the temperatures are high enough to trigger ionization of the species, the plasma field surrounding the body and even its wake can affect the aircraft's trackability and radio communications [1, 2].

This study uses Computational Fluid Dynamics to investigate the effects of high temperature in a sub-orbital hypersonic flight regime focusing on plasma formation prediction. The research concentrates on the effect of the number of species adopted to define the air mixture composition, investigating the sensitivity of the flow field to the adoption of 7-species or 11-species models. The simulations presented also use both reference thermo-chemical models [3, 4] and more recent versions incorporating kinetic parameters derived from shock tube experiments and state-to-state chemical kinetics [5]. With these models, we describe various combinations of Mach number and altitude conditions typical of atmospheric re-entry. We validate the results with experimental data collected from the RAM C-II test vehicle during its re-entry phase [6], and we perform a verification exercise by comparison with numerical simulations available in the literature [7].

2. Thermochemical Models

At sub-orbital altitudes, air can be modelled as a continuous flow governed by the Navier-Stokes equations for a multi-component gas mixture. At hypersonic speeds, however, this physical model must account for various non-equilibrium phenomena, including vibrational and electronic energy relaxation, dissociation and ionization. In this context, air is considered as a gas mixture consisting of several species. The 7-species model includes mono-atomic oxygen (O), mono-atomic nitrogen (N), nitrogen oxide (NO), diatomic oxygen (O_2), diatomic nitrogen (N_2), positive ions (NO^+) and electrons (e^-). In the extended 11 species model additional species such as O_2^+ , N_2^+ , O^+ and N^+ ions are considered. The two-temperature model is widely regarded as a good approximation for describing non-equilibrium phenomena in high-enthalpy and high-temperature gases [8]. In that model, the electron, electronic and vibrational energies are treated as a single non-equilibrium energy mode, known as the electron-electronic-vibrational energy, which evolves

Table 1: Reactions

Reactions	Third body	A [m ³ /kmol] Kim et al.	A [m ³ /kmol] Park et al	N _T Kim et al.	N _T Park et al.	T _f	T _b	
Dissociation reactions								
N ₂ + M ⇌ N + N + M	e ⁻	3.0 e21	3.0 e21	-1.6	-1.6	$\sqrt{TT_{v,e}}$	T	
	NO ⁺	7.0 e18	7.0 e18	-1.6	-1.6			
	N ⁺	3.591e17	3.0 e19	-1.226	-1.6			
	O ⁺	3.0 e19	3.0 e19	-1.6	-1.6			
	O ₂ ⁺	7.0 e18	7.0 e18	-1.6	-1.6			
	N ₂ ⁺	1.216 e17	7.0 e18	-1.214	-1.6			
	NO	7.0 e18	7.0 e18	-1.6	-1.6			
	N	3.591 e17	3.0 e19	-1.226	-1.6			
	O	3.0 e19	3.0 e19	-1.6	-1.6			
	O ₂	7.0 e18	7.0 e18	-1.6	-1.6			
	N ₂	1.216 e17	7.0 e18	-1.214	-1.6			
	O ₂ + M ⇌ O + O + M	NO ⁺	3.354 e12	2.0 e18	-0.2726			-1.5
		N ⁺	1.0 e19	1.0 e19	-1.5			-1.5
		O ⁺	3.0 e18	1.0 e19	-1.5			-1.5
O ₂ ⁺		1.117 e22	2.0 e18	-2.585	-1.5			
N ₂ ⁺		3.354 e12	2.0 e18	-0.2726	-1.5			
NO		3.354 e12	2.0 e18	-0.2726	-1.5			
N		1.0 e19	1.0 e19	-1.5	-1.5			
O		3.0 e18	1.0 e19	-1.5	-1.5			
O ₂		1.117 e22	2.0 e18	-2.585	-1.5			
N ₂		3.354 e12	2.0 e18	-0.2726	-1.5			
NO + M ⇌ N + O + M		NO ⁺	9.964 e11	5.0 e12	0.0	0.0		
		N ⁺	9.964 e11	1.1 e14	0.0	0.0		
		O ⁺	9.964 e11	1.1 e14	0.0	0.0		
		O ₂ ⁺	1.50 e12	5.0 e12	0.0	0.0		
	N ₂ ⁺	1.50 e12	5.0 e12	0.0	0.0			
	NO	9.964 e11	1.1 e14	0.0	0.0			
	N	9.964 e11	1.1 e14	0.0	0.0			
	O	9.964 e11	1.1 e14	0.0	0.0			
	O ₂	1.50 e12	5.0 e12	0.0	0.0			
	N ₂	1.50 e12	5.0 e12	0.0	0.0			
	Exchange reactions							
	NO + O ⇌ N + O ₂		8.4 e9	8.4 e9	0.0	0.0	T	T
	N ₂ + O ⇌ NO + N		5.7 e9	5.7 e9	0.42	0.42		
	Associative ionization reactions							
N + O ⇌ NO ⁺ + e ⁻		5.3 e9	5.3 e9	0.0	0.0	T	$\sqrt{TT_{v,e}}$	
O + O ⇌ O ₂ ⁺ + e ⁻		7.1 e-1	7.1 e-1	2.7	2.7			
N + N ⇌ N ₂ ⁺ + e ⁻		4.4 e4	4.4 e4	1.5	1.5			
Charge exchange reactions								
NO ⁺ + O ⇌ N ⁺ + O ₂		1.0 e9	1.0 e9	0.5	0.5	T	T	
N ⁺ + N ₂ ⇌ N ₂ ⁺ + N		1.0 e9	1.0 e9	0.5	0.5			
O ₂ ⁺ + N ⇌ N ⁺ + O ₂		8.7 e10	8.7 e10	0.14	0.14			
O ₂ ⁺ + NO ⇌ N ⁺ + O ₂		1.4 e2	1.4 e2	1.9	1.9			
O ₂ ⁺ + N ₂ ⇌ N ₂ ⁺ + O ₂		9.9 e9	9.9 e9	0.0	0.0			
O ₂ ⁺ + O ⇌ O ⁺ + O ₂		4.0 e9	8.4 e9	0.09	0.09			
NO ⁺ + N ⇌ O ⁺ + N ₂		3.4 e10	3.4 e10	-1.08	-1.08			
NO ⁺ + O ₂ ⇌ O ₂ ⁺ + NO		2.4 e10	2.4 e10	0.41	0.41			
NO ⁺ + O ⇌ O ₂ ⁺ + N		7.2 e10	7.2 e10	0.29	0.29			
O ⁺ + N ₂ ⇌ N ₂ ⁺ + O		9.1 e10	9.1 e10	0.36	0.36			
NO ⁺ + N ⇌ N ₂ ⁺ + O		7.2 e10	7.2 e10	0.0	0.0			
Electron-impact ionization reactions								
O + e ⁻ ⇌ O ⁺ + e ⁻ + e ⁻		3.9 e30	3.9 e30	-3.78	-3.78	T _{v,e}	T _{v,e}	
N + e ⁻ ⇌ N ⁺ + e ⁻ + e ⁻		2.5 e31	2.5 e31	-3.82	-3.82			

according to a balance equation that accounts for convection, diffusion and production/destruction. The electron-electronic-vibrational temperature, $T_{v,e}$, is used to describe this energy mode. On the other hand, the translational and rotational energies are assumed to be in equilibrium and are described by the roto-translational temperature, T . Chemical reactions involving dissociation, associative ionization and electron-impact ionization depend not only on the roto-translational temperature but also on the electronic-vibrational temperature.

The thermodynamic and diffusion properties of the individual species are obtained from the fittings presented in the work of Gupta et al. [9]. The forward rate constants are described by an Arrhenius-type relation:

$$k_{f,k} = A_k T^{N_T} e^{-\frac{E_{a,k}}{RT}} \quad (1)$$

In Equation (1), A_k represents the frequency factor of reaction k , $E_{a,k}$ is the activation energy, and N_T is the temperature exponent. The parameters in Equation (1) are derived from the widely adopted thermo-chemical model developed by Park [3, 4]. The backward reaction rates are determined by the equilibrium condition, which can be expressed as:

$$k_{b,k} = \frac{k_{f,k}(T_b)}{K_c(T)} \quad (2)$$

The equilibrium constants, K_c , are calculated based on the Gibbs free energies, as explained in Anderson [10]. The backward and forward rate constants are computed using temperatures denoted as T_f and T_b , respectively, which account for the energy states of the reacting species. These temperatures can be either the translational-rotational temperature T , the vibrational-electronic temperature $T_{v,e}$, or a combination of the two. For more detailed information regarding the chemical reactions and characteristic temperatures, please refer to Table 1.

Recent advances in shock tube experiments have revealed discrepancies with the kinetic parameters of the Park model [3, 4]. These inaccuracies arise from the fact that most chemical kinetics parameters defined in the early 1990s were based on limited temperature ranges, specifically up to 5000K in shock tube experiments. However, more recent studies of the state-to-state chemical kinetics of atmospheric gases have addressed the challenges posed by the inaccuracy of the older chemical reaction rates. These studies use ab initio calculated potential energy surfaces and compare the results with shock tube experiments at much higher translational temperatures than in the past. For the second model we consider, the values of the forward rate constants for the dissociation reactions are chosen based on fits from recent studies proposed by Kim and Jo [5]. Specifically, for the dissociation reaction with reactants $N_2 + N_2$, the reaction rates obtained from state-to-state chemical kinetics investigations presented by Bender et al. [11] and Jaffe et al. [12] agree well with results from shock tube experiments at temperatures below 14000 degrees [13, 14, 15, 16]. Similarly, for the dissociation reaction with reactants $N_2 + N$, the reaction rates calculated by Kim and Boyd using state-to-state kinetics [17] were found to be in good agreement with the experimental measurements described in [18]. In the case of the dissociation of O_2 , the reaction rates for the reactions involving the reactants $O_2 + N_2$, $O_2 + O_2$ and $O_2 + O$ are based on the state-to-state kinetic calculations presented in Kim et al. [19], which show good agreement with the results from detonated shock tube measurements presented in [20, 21]. The dissociation of NO is based on the reaction rates presented by Tsang and Herron [22], who take into account some uncertainty in the atomic resonance absorption spectroscopy measurements mentioned in [23] and propose a corrective factor. Estimation of reaction rates for collision-induced dissociation of charged particles is difficult because these collisions are less significant than those involving neutral particles in hypersonic flows. Therefore, the same values used for neutral collisions are adopted. The reaction rates of the Park model [3, 4] govern the other types of reaction. Bold characters in Table 1 help to identify those Arrhenius coefficients that differ between the Park [3, 4] and the Kim and Jo [5] model.

3. Numerical Method

The governing equations are numerically solved using the CFD software ICFD++ developed by Metacomp Technologies [24]. The CFD code employs a finite volume discretization and utilizes an HLLC approximate Riemann solver with TVD-limited second-order reconstruction for convective fluxes. Diffusive fluxes are calculated using a centered, naturally second-order scheme [25, 26, 27, 28]. Since we are considering a simplified geometric representation of the RAM C-II vehicle, assuming an axially symmetric body as in Fig.1a and analyzing conditions at zero angle of attack,

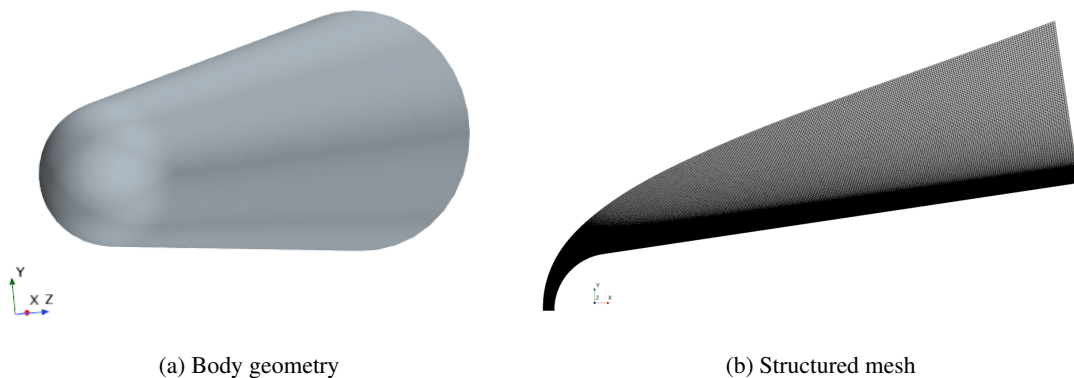


Figure 1: RAMC-II representative body and related axisymmetric mesh.

we can treat the flow field as axisymmetric. The computational mesh (Fig.1b) contains approximately 170,000 quadrilateral cells for the considered test cases. For these 2D-axisymmetric simulations, such a number of cells is sufficient to ensure grid convergence. The mesh is stretched at the wall to ensure that the boundary layer is accurately captured.

The blunt axisymmetric cone representing the RAM C-II is subjected to hypersonic flow at various Mach numbers and altitudes typically encountered during atmospheric reentry. The numerical simulations assume laminar conditions, except for the case at Mach 23.9 and 61 km altitude, where we adopt the Reynolds-averaged Navier-Stokes (RANS) equations in combination with the SST $k - \omega$ turbulence model proposed by Menter [29]. The characteristic convective time t_c , defined as the body length divided by the freestream velocity, is of the order of magnitude of 10^{-4} s for the considered conditions. The governing equations are solved using a second-order implicit time-dependent scheme with a time step $\Delta t = 5 \cdot 10^{-6}$ s. Each simulation runs until the residuals decrease by six orders of magnitude compared to the initial time step, which we assume to be a condition very close to the steady state. Depending on the specific test case, that typically occurs after 40,000 to 50,000 time steps.

4. Results

In the following subsections, we present the results obtained from two chemical kinetics models. One model utilizes the forward reaction rates proposed by Park [3, 4], while the other model employs the forward reaction rates suggested by Kim and Jo [5]. We conducted these simulations using different numbers of species to represent the mixture, specifically a 7-species model and an 11-species model. Therefore, we have a total of four chemical kinetic models available for comparison.

For our analysis, we considered three freestream conditions as listed in Table 2, which are relevant to the reentry phase of the RAM C-II. The wall is assumed to be non-catalytic and has a fixed temperature ($T_w = 1000K$).

test case #	Mach number	altitude [km]	lam/turb
# 1	23.9	61	turbulent
# 2	25.9	71	laminar
# 3	28.3	81	laminar

Table 2: The considered test case conditions.

The neutral species values along the stagnation axis of the aircraft are compared with other numerical results [7], and the maximum electron number density values at different axial positions are validated using experimental measurements from reflectometers and electrostatic probes placed along the body [6]. The probe positions are listed in Fig.2a and illustrated in Fig.2b.

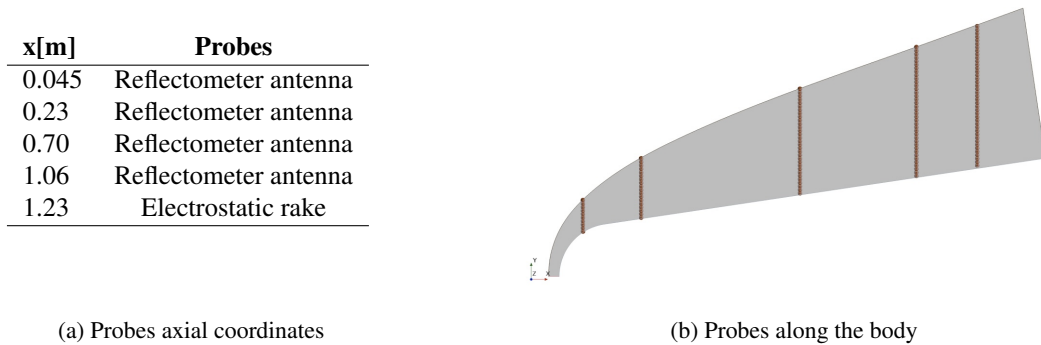
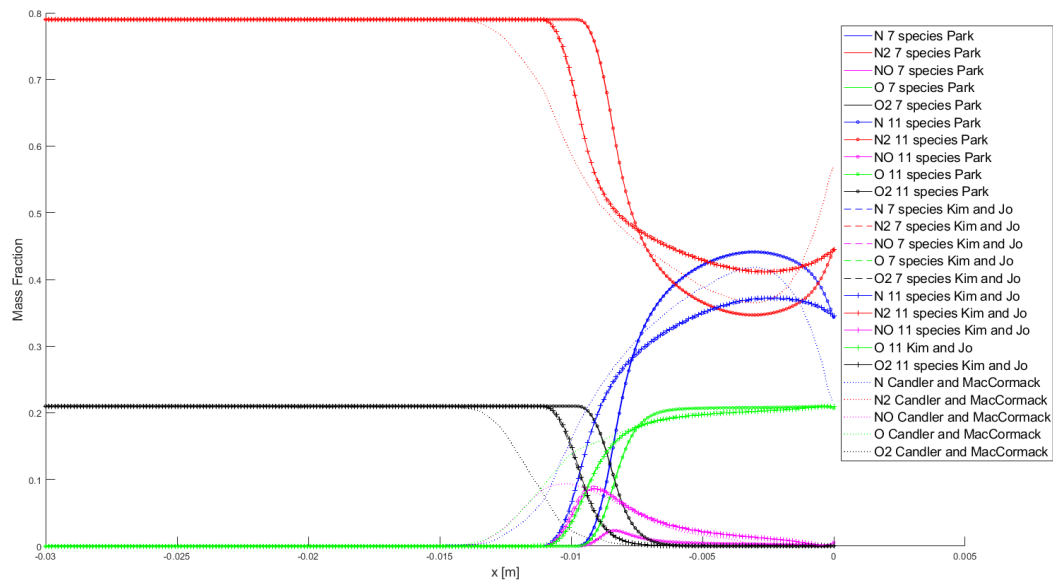


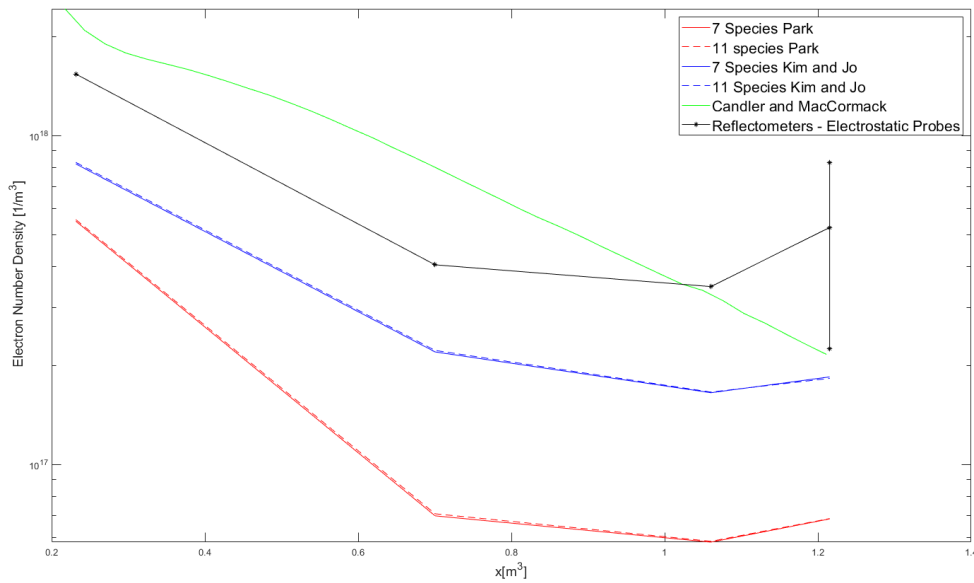
Figure 2: Probes positions along the body

4.1 Results at Mach 23.9 and 61 km altitude

Significant chemical activity is observed on the nose of the vehicle due to higher temperatures, as clearly visible in Fig.3a. Oxygen dissociation occurs rapidly across the shock wave and quickly completes. However, nitrogen dissociation is only partial, which is typical during Earth entry. Analyzing Fig.3a and Fig.3b reveals no significant differences along the stagnation axis between 7- and the 11-species models. The differences in the N_2 concentrations between the Park and the Kim and Jo model likely contribute to the difference in the shock stand-off distance. More



(a) Mass fraction along the stagnation line.



(b) Maximum electron number density at various stations along the body.

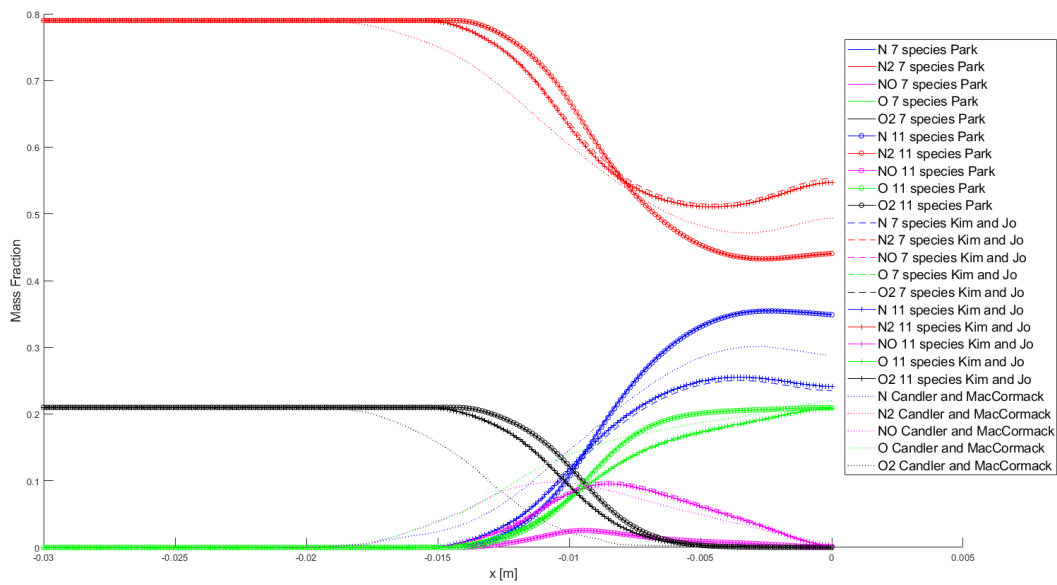
Figure 3: Results for Mach 23.9 and 61 km altitude.

N_2 dissociation leads to lower temperatures, resulting in higher density and a shock wave closer to the body. When comparing with the numerical results of Candler and MacCormack [7], the Park model tends to overestimate nitrogen dissociation, while the Kim and Jo model slightly underestimates it. However, the Kim and Jo model aligns with Candler and MacCormack's results in terms of the order of magnitude of the maximum NO mass fraction. Notably, there is a noticeable disparity in the stand-off distance, with Candler and MacCormack's results showing a larger stand-off distance compared to all our results. Several factors contribute to these discrepancies. Firstly, while Candler and MacCormack [7] rely on the fitting suggested by Park [30], our model evaluates equilibrium constants using Gibbs free energies. The effect is clearly visible in the concentrations of N_2 and N at the wall, where equilibrium conditions are reached. Secondly, the backward temperatures used in our model differ from those employed by Candler and MacCormack. Thirdly, in this specific test case, we are using a turbulence model, while Candler and MacCormack

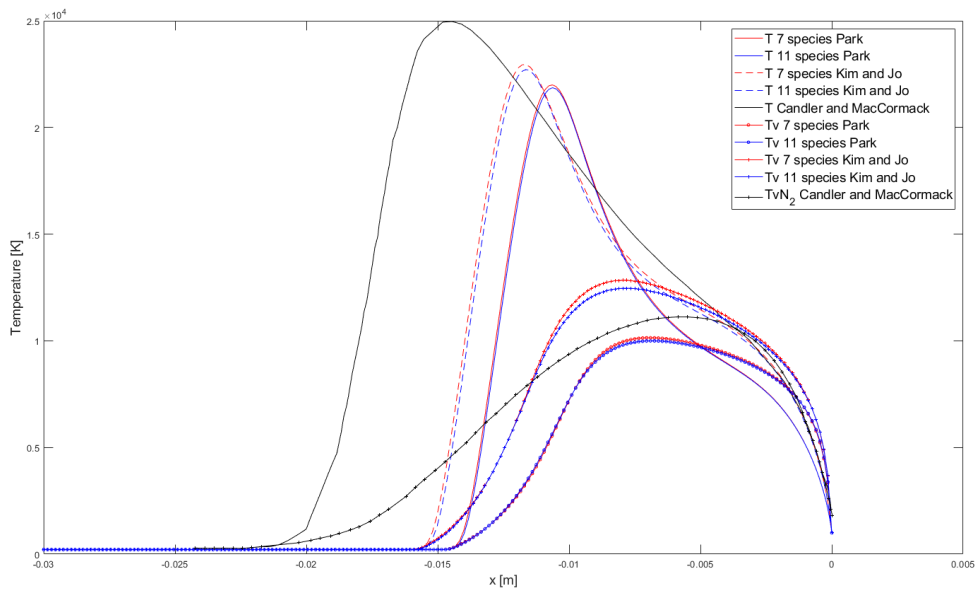
assume laminar flow. Lastly, our grid has a significantly finer resolution, resulting in a more accurate and less diffused capture of the shock wave. Regarding plasma measurements, upon examining Fig.3b, it is apparent that the model based on Kim and Jo's chemical kinetic parameters demonstrates closer alignment with the experimental measurements.

4.2 Results at Mach 25.9 and 71 km altitude

Compared to the previous case, the chemical relaxation appears more diffuse, as shown in Fig.4a. That is primarily due to the lower density and pressure at that altitude. Similar to the previous case, there appear to be no significant differences on the stagnation axis resulting from the adoption of the 7- or the 11-species model. However, we observe



(a) Mass fractions along the stagnation line.



(b) Temperatures distributions along the stagnation line.

Figure 4: Results at Mach 25.9 and 71 km altitude.

discrepancies similar to those noticed at lower altitudes between the results obtained using the Park and the Kim and Jo models. The Kim and Jo model predicts less pronounced nitrogen dissociation compared to the Park model, which also predicts a lower peak in NO production. Once again, the results by Candler and MacCormack display a larger stand-off distance. Fig.4b illustrates the temperature distributions along the stagnation axis for the different models we tested and the results from Candler and MacCormack. It is important to underline that the modelling of internal energy differs noticeably between our approach and that of Candler and MacCormack. The latter employs a multi-temperature model with distinct non-equilibrium balance equations for the vibrational energies of each diatomic species and an electron energy balance equation. Moreover, the energy exchange mechanisms in the Candler and MacCormack model are more accurate than those in our adopted model, as they account not only for vibration-translation energy exchanges but also for vibration-vibration, translation-electron, and electron-vibration energy exchanges. Considering Fig.4b, one immediate observation is that Candler and MacCormack's results show a higher temperature peak in the post-shock region compared to our results. That is due to the fact that all relaxation phenomena in the Candler and MacCormack data appear to occur at a slower pace than in our results, regardless of the model we adopt. Although all temperatures converge to the boundary value at the wall, the species concentrations at the wall in our models are different, suggesting that equilibrium was not reached. This is a puzzling outcome that will require further verification in the future. One possibility is that the time required to reach equilibrium close to the stagnation point in these low-density conditions is very long compared to other characteristic times, and we may not have run the simulations for a sufficient duration. Another possibility is that in these low-density conditions, equilibrium at the wall is achieved within an extremely thin layer that is not adequately resolved by the mesh we are using.

Regarding the electron number density along the body, it is worth noting that the results exhibit heightened sensitivity to the adoption of a 7-species or 11-species model, as evident from the electron concentrations in Fig.5. Interestingly, a model utilizing a mixture of 11 species yields superior results compared to the model with only 7 species. All results presented in Fig. 5 maintain consistency with the evaluation of electron number density conducted by Candler and MacCormack [7]. Overall, the results presented in Fig.4 and 5 indicate that using an 11-species model and the reaction rates by Kim and Jo provide numerical results that align better with experimental and numerical data.

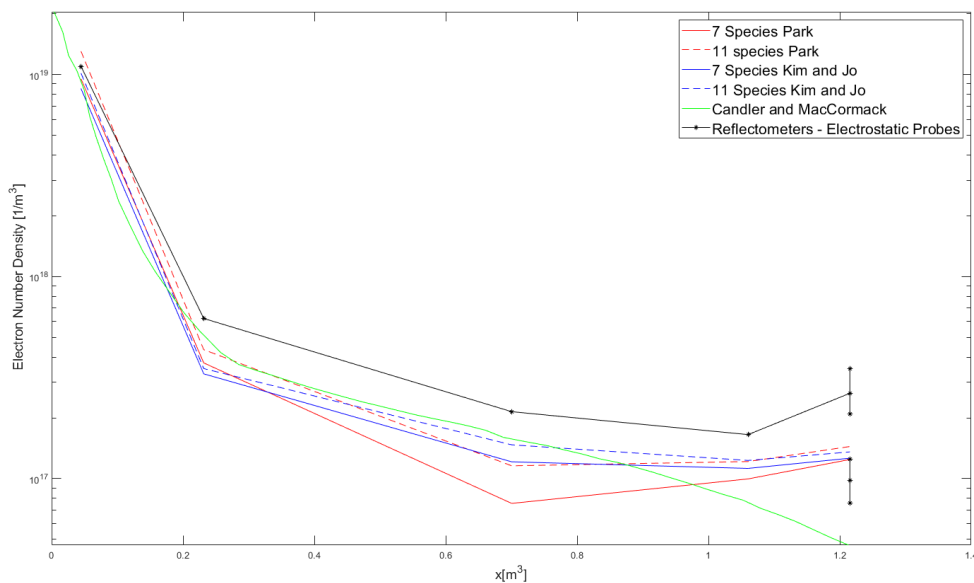
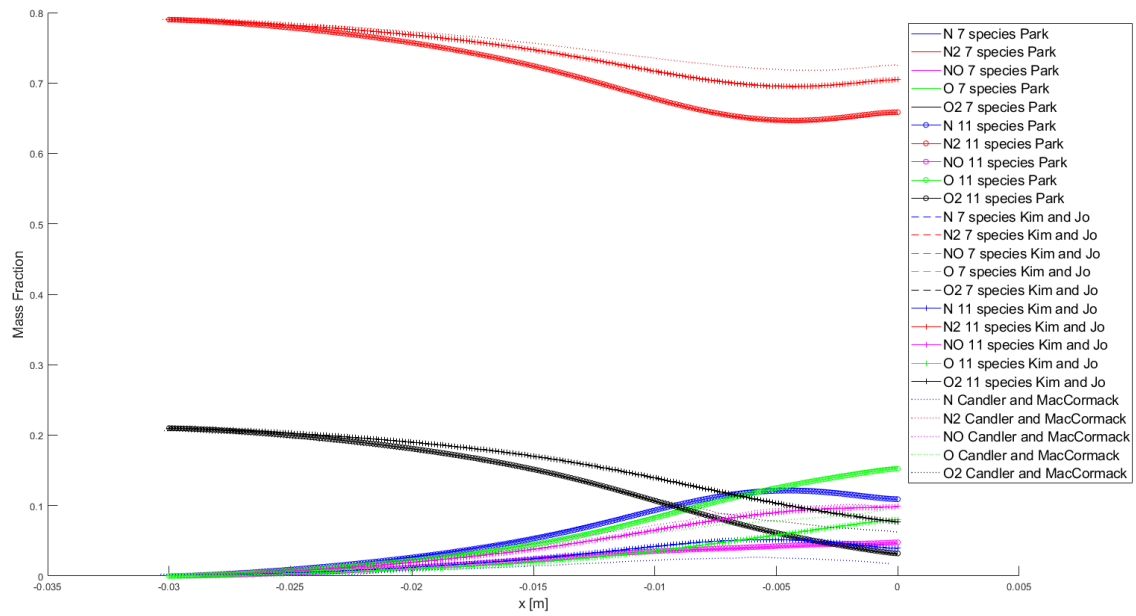


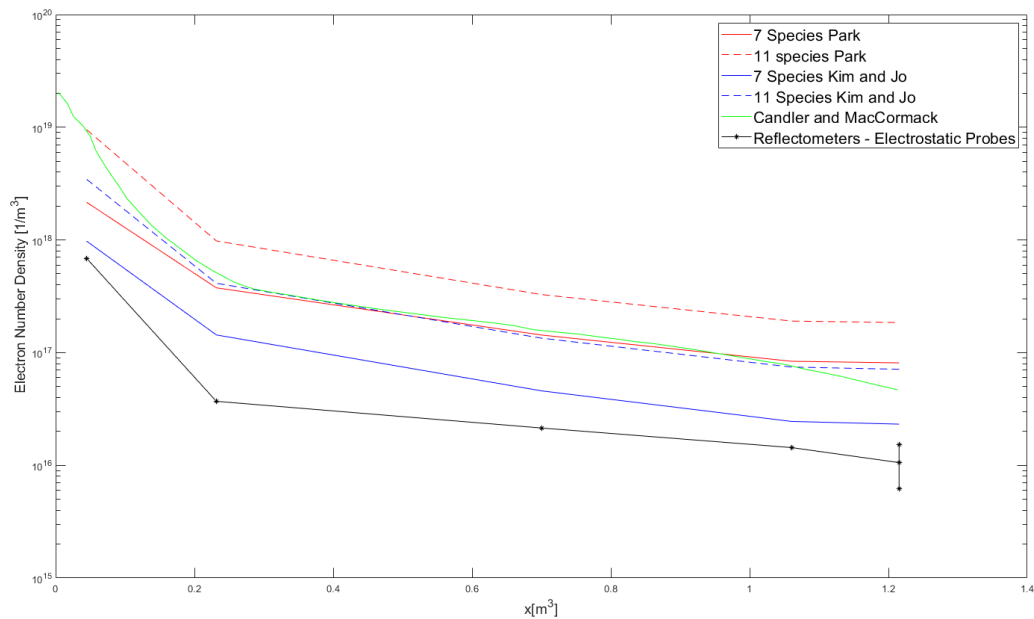
Figure 5: Maximum electron number density at various stations along the body at Mach 25.9 and 71 km altitude.

4.3 Results at Mach 28.3 and 81 km altitude

In the last considered flight condition, as shown in Fig.6a, it is immediately apparent that the thermo-chemical activity is significantly diminished compared to conditions at lower altitudes. Differences in results along the stagnation axis persist consistently. The shock wave is further diffused due to the reduced density. Even oxygen does not reach a state of chemical equilibrium due to the limited number of collisions at that altitude. Fig.6b illustrates how the differences among the various models are notably pronounced when it comes to the electron concentration along the body. The



(a) Mass fractions along the stagnation line.



(b) Maximum electron number density at various stations along the body.

Figure 6: Results at Mach 28.3 and 81 km altitude.

results for an air composition with 7 species appear to be closer to the experimental data than those for an 11-species gas mixture. However, an 11-species air mixture composition with the Kim and Jo model closely aligns with the numerical reference data from Candler and MacCormack [7]. While the trends follow the experimental findings, the thermo-chemical model based on the forward reaction rates of Kim and Jo presents better results than the others in all previously examined cases, but only when air is considered a 7-species gas mixture.

5. Conclusions

The primary objective of this study was to conduct a comparative analysis between two chemical kinetics models: the widely used Park model and a recent model by Kim and Jo that incorporates reaction rate parameters obtained from shock tube experiments and state-to-state chemistry studies. Additionally, we evaluated the models' sensitivity to mixture composition by conducting simulations using high-temperature air consisting of 7 and 11 species.

The results obtained from the CFD simulations were analyzed at three trajectory points relevant to the reentry conditions of the RAM C-II flying experiment. No significant differences were observed between the 7 and 11-species models in the stagnation region. However, the results obtained with the Kim and Jo model demonstrated better agreement with the numerical data available in the literature.

Regarding the electron concentration, there were no notable differences based on the choice of mixture composition at an altitude of 61 km. At higher altitudes, where thermo-chemical activity decreases due to lower pressures and densities, the mixture composition was found to have a significant impact on the flow field. Results obtained at the 71 km and 81 km altitudes suggest that the 11-species model generally provides a more accurate representation compared to experimental data. For each altitude, the model incorporating more recent data exhibited a closer resemblance when compared to both numerical and experimental result

6. Acknowledgments

This research was conducted in part under the financial support provided by the PON (Programmi Operativi Nazionali) research funds. We are grateful to the Italian Ministry of Education, University and Research (MIUR) for managing the PON funding program and for supporting our research endeavors.

References

- [1] P. A. Gnoffo, "Planetary-entry gas dynamics," *Annual Review of Fluid Mechanics*, vol. 31, no. 1, pp. 459–494, 1999.
- [2] T. H. Stix, *Waves in plasmas*. Springer Science & Business Media, 1992.
- [3] C. Park, "Review of chemical-kinetic problems of future NASA missions. I-Earth entries," *Journal of Thermophysics and Heat transfer*, vol. 7, no. 3, pp. 385–398, 1993.
- [4] C. Park, R. L. Jaffe, and H. Partridge, "Chemical-kinetic parameters of hyperbolic Earth entry," *Journal of Thermophysics and Heat transfer*, vol. 15, no. 1, pp. 76–90, 2001.
- [5] J. G. Kim and S. M. Jo, "Modification of chemical-kinetic parameters for 11-air species in re-entry flows," *International Journal of Heat and Mass Transfer*, vol. 169, p. 120950, 2021.
- [6] W. L. Jones and A. E. Cross, "Electrostatic-probe measurements of plasma parameters for two reentry flight experiments at 25000 feet per second," NASA TN D-6617, 1972.
- [7] G. V. Candler and R. W. MacCormack, "Computation of weakly ionized hypersonic flows in thermochemical nonequilibrium," *Journal of Thermophysics and Heat Transfer*, vol. 5, no. 3, pp. 266–273, 1991.
- [8] C. Park, "Assessment of two-temperature kinetic model for ionizing air," *Journal of Thermophysics and Heat Transfer*, vol. 3, no. 3, pp. 233–244, 1989.
- [9] R. N. Gupta, J. M. Yos, R. A. Thompson, and K.-P. Lee, "A review of reaction rates and thermodynamic and transport properties for an 11-species air model for chemical and thermal nonequilibrium calculations to 30000 K," NASA-TR-1232, 1990.
- [10] J. D. Anderson, *Hypersonic and High-Temperature Gas Dynamics*. AIAA Educational Series, Third Edition ed., 2019.
- [11] J. D. Bender, P. Valentini, I. Nompelis, Y. Paukku, Z. Varga, D. G. Truhlar, T. Schwartzentruber, and G. V. Candler, "An improved potential energy surface and multi-temperature quasiclassical trajectory calculations of $N_2 + N_2$ dissociation reactions," *The Journal of Chemical Physics*, vol. 143, p. 054304, 08 2015.

- [12] R. L. Jaffe, M. Grover, S. Venturi, D. W. Schwenke, P. Valentini, T. E. Schwartzentruber, and M. Panesi, "Comparison of potential energy surface and computed rate coefficients for N_2 dissociation," *Journal of Thermophysics and Heat Transfer*, vol. 32, no. 4, pp. 869–881, 2018.
- [13] B. Cary, "Shock-tube study of the thermal dissociation of nitrogen," *The Physics of Fluids*, vol. 8, no. 1, pp. 26–35, 1965.
- [14] S. Byron, "Shock-tube measurement of the rate of dissociation of nitrogen," *The Journal of Chemical Physics*, vol. 44, no. 4, pp. 1378–1388, 1966.
- [15] J. Appleton, M. Steinberg, and D. Liquornik, "Shock-tube study of nitrogen dissociation using vacuum-ultraviolet light absorption," *The Journal of Chemical Physics*, vol. 48, no. 2, pp. 599–608, 1968.
- [16] R. K. Hanson and D. Baganoff, "Shock-tube study of nitrogen dissociation rates using pressure measurements," *AIAA Journal*, vol. 10, no. 2, pp. 211–215, 1972.
- [17] J. G. Kim and I. D. Boyd, "State-resolved master equation analysis of thermochemical nonequilibrium of nitrogen," *Chemical Physics*, vol. 415, pp. 237–246, 2013.
- [18] J. G. Kim and I. D. Boyd, "Master equation analysis of post normal shock waves of nitrogen," *Journal of Thermophysics and Heat Transfer*, vol. 29, no. 2, pp. 241–252, 2015.
- [19] J. G. Kim, S. H. Kang, and S. H. Park, "Thermochemical nonequilibrium modeling of oxygen in hypersonic air flows," *International Journal of Heat and Mass Transfer*, vol. 148, p. 119059, 2020.
- [20] L. B. Ibraguimova, A. L. Sergievskaya, V. Y. Levashov, O. P. Shatalov, Y. V. Tunik, and I. E. Zabelinskii, "Investigation of oxygen dissociation and vibrational relaxation at temperatures 4000-10800 K," *The Journal of Chemical Physics*, vol. 139, p. 034317, 07 2013.
- [21] L. Ibraguimova, A. Sergievskaya, and O. Shatalov, "Dissociation rate constants for oxygen at temperatures up to 11000 K," *Fluid Dynamics*, vol. 48, pp. 550–555, 2013.
- [22] W. Tsang and J. T. Herron, "Chemical Kinetic Data Base for Propellant Combustion I. Reactions Involving NO, NO₂, HNO, HNO₂, HCN and N₂O," *Journal of Physical and Chemical Reference Data*, vol. 20, no. 4, pp. 609–663, 1991.
- [23] K. Thielen and P. Roth, "Resonance absorption measurements of N and O atoms in high temperature NO dissociation and formation kinetics," in *Symposium (International) on Combustion*, vol. 20, pp. 685–693, Elsevier, 1985.
- [24] S. Chakravarthy, O. Perroomian, U. Goldberg, and S. Palaniswamy, "The CFD++ Computational Fluid Dynamics Software Suite," in *AIAA and SAE, 1998 World Aviation Conference*, (Anheim, CA), 1998. AIAA-1998-5564.
- [25] S. Chakravarthy, O. Perroomian, and B. Sekar, "Some internal flow applications of a unified-grid CFD methodology," in *32nd Joint Propulsion Conference and Exhibit*, (Lake Buena Vista, FL), 1996. AIAA-1996-2926.
- [26] O. Perroomian, S. Chakravarthy, U. Goldberg, O. Perroomian, S. Chakravarthy, and U. Goldberg, "A 'grid-transparent' methodology for CFD," in *35th Aerospace Sciences Meeting and Exhibit*, (Reno, NV), 1997. AIAA-1997-0724.
- [27] O. Perroomian, S. Chakravarthy, S. Palaniswamy, and U. Goldberg, "Convergence acceleration for unified-grid formulation using preconditioned implicit relaxation," in *36th AIAA Aerospace Sciences Meeting and Exhibit*, (Reno, NV), 1998. AIAA-1998-0116.
- [28] P. Batten, M. A. Leschziner, and U. Goldberg, "Average-state jacobians and implicit methods for compressible viscous and turbulent flows," *Journal of computational physics*, vol. 137, no. 1, pp. 38–78, 1997.
- [29] F. R. Menter, "Improved two-equation k-omega turbulence models for aerodynamic flows," NASA-TM-103975, 1992.
- [30] C. Park, "On convergence of computation of chemically reacting flows," in *23rd Aerospace Sciences Meeting*, (Reno, NV), 1985. AIAA-1995-0247.